

Calcium Oscillations in a Triplet of Pancreatic Acinar Cells

K. Tsaneva-Atanasova,* D. I. Yule,[†] and J. Sneyd[‡]

*Department of Mathematics, University of Auckland, New Zealand; [†]Department of Pharmacology and Physiology, University of Rochester, Medical Center, Rochester, New York; and [‡]Department of Mathematics, University of Auckland, New Zealand

ABSTRACT We use a mathematical model of calcium dynamics in pancreatic acinar cells to investigate calcium oscillations in a ring of three coupled cells. A connected group of cells is modeled in two different ways: 1), as coupled point oscillators, each oscillator being described by a spatially homogeneous model; and 2), as spatially distributed cells coupled along their common boundaries by gap-junctional diffusion of inositol trisphosphate and/or calcium. We show that, although the point-oscillator model gives a reasonably accurate general picture, the behavior of the spatially distributed cells cannot always be predicted from the simpler analysis; spatially distributed diffusion and cell geometry both play important roles in determining behavior. In particular, oscillations in which two cells are in synchrony, with the third phase-locked but not synchronous, appears to be more dominant in the spatially distributed model than in the point-oscillator model. In both types of model, intercellular coupling leads to a variety of synchronous, phase-locked, or asynchronous behaviors. For some parameter values there are multiple, simultaneous stable types of oscillation. We predict 1), that intercellular calcium diffusion is necessary and sufficient to coordinate the responses in neighboring cells; 2), that the function of intercellular inositol trisphosphate diffusion is to smooth out any concentration differences between the cells, thus making it easier for the diffusion of calcium to synchronize the oscillations; 3), that groups of coupled cells will tend to respond in a clumped manner, with groups of synchronized cells, rather than with regular phase-locked periodic intercellular waves; and 4), that enzyme secretion is maximized by the presence of a pacemaker cell in each cluster which drives the other cells at a frequency greater than their intrinsic frequency.

INTRODUCTION

The rise of the cytosolic calcium concentration in response to agonist stimulation is widely believed to be a key event underlying the secretion of digestive enzymes in pancreatic acinar cells (Kasai, 1995; Wäslé and Edwardson, 2002). Ca^{2+} release induced by inositol trisphosphate (IP_3) generally takes the shape of $[\text{Ca}^{2+}]_i$ oscillations, the period and amplitude of which depend on the agonist concentration. In pancreatic acinar cells Ca^{2+} waves are generally initiated in the apical region and spread over the cell to form a global intracellular wave (Fogarty et al., 2000b; Nathanson et al., 1992; Straub et al., 2000). Moreover, this Ca^{2+} wave can propagate from one cell to another. Similar intercellular Ca^{2+} waves have been reported in a wide range of different cell types, such as airway epithelial cells (Sanderson, 1995), astrocytes (Giaume and Venance, 1998), and in the intact liver (Thomas et al., 1995; Robb-Gaspers and Thomas, 1995). In a pancreatic acinus, Ca^{2+} signals appear to travel in a wavelike manner between coupled cells and thereby serve as a means of intercellular communication (Petersen and Petersen, 1991; Stauffer et al., 1993; Yule et al., 1996).

Intercellular Ca^{2+} waves have been extensively studied in other cell types. Early models of intercellular Ca^{2+} waves in epithelial cells (Sneyd et al., 1995) proposed the intercellular diffusion of IP_3 as the principal wave-generating mechanism, whereas recent experimental work has pointed out the im-

portance of extracellular diffusing messengers, at least in some cell types (Clair et al., 2001; Yule et al., 1996). Two recent studies by G. Dupont and her colleagues (Clair et al., 2001; Dupont et al., 2000a, 2000b), and T. Höfer (Höfer, 1999; Höfer et al., 2001) have been published on multiplets of hepatocytes, the former maintaining the crucial importance of IP_3 as a signaling messenger and the latter showing that junctional Ca^{2+} diffusion is the most significant for synchronization. These studies in hepatocytes are not yet satisfactorily resolved. However, one thing of which we are certain is that a single model cannot possibly hope to be appropriate for all cell types in which such intercellular waves are observed. Despite this, models tend to explain the coordination of intercellular waves by a combination of one or more of three general mechanisms: 1), the diffusion of Ca^{2+} through gap junctions; 2), the diffusion of IP_3 through gap junctions; and 3), an extracellular diffusing messenger.

It is our goal to determine the principal mechanisms by which intercellular waves in pancreatic acinar cells are coordinated. Acinar cells are known to be connected by gap junctions (Ngezahayo and Kolb, 1993; Petersen and Petersen, 1991; Stauffer et al., 1993; Yule et al., 1996), and it has been claimed that the intercellular diffusion of Ca^{2+} and/or IP_3 could be important mechanisms by which a group of acinar cells could coordinate their responses (Ngezahayo and Kolb, 1993; Petersen and Petersen, 1991; Stauffer et al., 1993; Yule et al., 1996). Furthermore it has been suggested that transmission of the signal from the most agonist-sensitive cells to the neighboring cells could explain

Submitted June 8, 2004, and accepted for publication November 23, 2004.

Address reprint requests to J. Sneyd, Fax: 64-9-3737-457; E-mail: sneyd@math.auckland.ac.nz.

© 2005 by the Biophysical Society

0006-3495/05/03/1535/17 \$2.00

doi: 10.1529/biophysj.104.047357

why preparations of acini secrete digestive enzymes more efficiently than single cells (Yule et al., 1996). Intriguingly, increasing the frequency of the Ca^{2+} oscillations by modulation of gap-junctional permeability appears to increase the rate of enzyme secretion (Stauffer et al., 1993). However, despite numerous experimental studies, the precise role of either Ca^{2+} or IP_3 diffusion remains unclear.

Yule et al. (1996) investigated intercellular Ca^{2+} signaling in connected clusters of acinar cells. Their observations can be briefly described as follows:

1. The spatial and temporal characteristics of the Ca^{2+} signal are dependent on the level of agonist stimulation. A stimulation with low concentration of agonist results in coordinated increases in $[\text{Ca}^{2+}]$ in individual coupled cells. In particular the spike initiated in one of the cells in a triplet spreads to the second, and later the third cell, followed by a rest period. A further cycle regenerates from the same cell as the first spike and propagates in a similar manner. At high agonist concentration, a synchronous rise in $[\text{Ca}^{2+}]$ in all cells of the acinus was observed.
2. Injection of IP_3 into one cell in an acinar cluster can initiate an increase in $[\text{Ca}^{2+}]$ not only in that cell but also in adjacent neighbors, a finding that indicates strongly that molecule(s) capable of modulating Ca^{2+} signaling can diffuse between coupled cells.
3. Addition of Ca^{2+} by itself is not sufficient to initiate wave propagation in adjacent cells.
4. Injection of antagonist (heparin) into a single cell abolishes Ca^{2+} oscillations in that cell, which suggests that IP_3 plays an integral role in intercellular as well as intracellular signaling and reinforces the view that elevated $[\text{Ca}^{2+}]$ in one cell is not capable, in isolation, of triggering an increase in Ca^{2+} concentration in neighboring cells.
5. In contrast to CaCl_2 injection in the absence of a background elevation in $[\text{IP}_3]$, CaCl_2 injection while IP_3 is simultaneously elevated by agonist stimulation results in the augmentation of the Ca^{2+} signal in the injected cell's neighbors.

Based on these data, it was proposed that Ca^{2+} acts as a co-agonist with IP_3 to enhance the Ca^{2+} -releasing action of IP_3 receptors and that diffusion of the two molecules through gap junctions underlie intercellular signaling in acinar cells.

Some of these results were studied by Sneyd et al. (2003), whereas others we have checked in the present work. However, we do not show detailed pictures of those results here. Essentially, given the fact that the model was constructed precisely to behave in this manner, the fact that it can qualitatively reproduce those results comes as no surprise, and tells us little about the cells that we did not already know. Here, instead, we study a much more complex and less well-understood problem—that of intercellular synchronization, which was the subject of point 1, above.

Our study is based on the previous model of Ca^{2+} dynamics in pancreatic acinar cells due to Sneyd et al. (2003), which we describe in detail in Appendix 1. From this model we construct two qualitatively different models of a triplet of coupled acinar cells.

Model 1: point oscillators

We begin by modeling a triplet of cells as a system of three coupled oscillators. Each oscillator is described by a purely temporal model with no spatial gradients of Ca^{2+} or IP_3 (i.e., a system of ordinary differential equations). The cells are coupled by transmembrane diffusion of Ca^{2+} or IP_3 , or both. We perform a bifurcation analysis of this coupled system of ordinary differential equations and describe the various possible kinds of oscillations that occur in such a triplet of coupled oscillators. Our results here are generic; there is nothing special about pancreatic cell oscillators to distinguish them from any other triplet of coupled oscillators. Nevertheless, the exact behavior must be established before the results can be compared to the spatially distributed model.

Model 2: spatially distributed cells

Next, we construct a spatially distributed version of the model, in which each cell is modeled as a two-dimensional continuum, coupled to its neighbors along each common border. This model thus uses partial differential equations and is solved numerically using a finite element method. The various oscillatory modes that appear are complicated by the nature of the oscillation within each individual cell. Nevertheless, useful comparisons can be made to the point-oscillator model. In effect, the spatially distributed model provides an important check on whether the point-oscillator model can say anything useful about the actual physiological system.

Using these two models,

1. We investigated the importance of intercellular diffusion of IP_3 and Ca^{2+} for the coordination of intercellular oscillations. We found that intercellular diffusion of IP_3 was insufficient to generate phase-locked waves, whereas intercellular diffusion of Ca^{2+} was necessary and sufficient. However, it is important to realize that this conclusion is dependent on our model assumptions, as we discuss later. Use of a different model for the cellular IP_3 dynamics could well result in a different conclusion.
2. We evaluated the importance of the relative differences between concentrations of IP_3 among connected cells. Our results indicate that, the smaller the differences in $[\text{IP}_3]$ between the cells, the easier it is for Ca^{2+} diffusion to phase-lock the responses. Thus we predict that the function of intercellular diffusion of IP_3 is to minimize the intercellular concentration gradients of IP_3 , thus

making it easier for Ca^{2+} diffusion to phase-lock the responses.

3. We analyzed the possible modes of synchronization among three coupled cells. In the point-oscillator model we found most of the usual types of synchrony and phase-locking that are well known from other coupled oscillator systems (Strogatz and Stewart, 1993). However, we found that the stability of each of these modes was different in the two models. Most interestingly, we found that in the spatially distributed model the most stable phase-locked mode was one where two cells oscillate in synchrony, with the third cell phase-locked but with a different phase. The phase-locked oscillation in which each cell is exactly $1/3$ out of phase was not a stable solution for the spatially distributed model, although it was stable in the point-oscillator model. Our model thus predicts that regular intercellular waves, moving at constant speed around a ring of cells, would not, in general, be observed.
4. We estimated the significance of heterogeneities in structural properties such as cell size and shape, or differences in IP_3 production, which may account for gradients of the intrinsic oscillation frequencies of cells. It is clear that cell geometry plays an important role that cannot be ignored. It is not yet clear how much our results depend on the exact geometry we used. Resolution of that question awaits detailed simulations on a range of complex multicellular geometries.
5. We analyzed the role of a pacemaker cell in a cluster of three cells. We found that the cell with the highest natural oscillation frequency will usually act as the pacemaker, driving the other cells to oscillate at frequencies higher than their normal frequency. Thus our results predict that the role of gap junctions in maximizing enzyme secretion is precisely to enable the emergence of a pacemaker.

For the readers' convenience, we summarize the terminology we use here as

Synchronized oscillations are where the cells are oscillating with identical phases (i.e., a phase difference $\tau = 0$ between the cells).

Phase-locked oscillations are where the phase difference is non-zero but constant.

Symmetric phase-locked oscillations are where the phase difference between each pair of neighboring cells is the same. For instance, in the case of three cells, the phase difference between any two cells would be $1/3$ of the period.

Asymmetric phase-locked oscillations are phase-locked but with no regular difference in phase between pairs of neighboring cells.

Asynchronous oscillations are where there is no relationship between the phases of the oscillatory responses in the three cells.

MODEL 1: POINT-OSCILLATOR CELLS

We begin by discussing the first model, the point-oscillator model. Of course, such a simplified model bears little resemblance to the actual physiological situation in which the cells are clearly spatially distributed. Despite this, we wish to discover just how much of the behavior of this simple model carries over to the more complicated case, and whether any insight can be gained from such a drastic (although commonly used) simplification.

Description of the model

We approximate a cluster of three pancreatic acinar cells with a bi-directional ring of three identical, symmetrically and diffusively coupled oscillators. A schematic diagram of Model 1 is presented in Fig. 1 A. The model for the dynamics of each cell in the cluster is based on a recent model of intracellular Ca^{2+} dynamics in pancreatic acinar cells, published by Sneyd et al. (2003). Although, in the original model, the cell was assumed to have distinct apical and basal regions, with parameter values that were determined by fitting to experimental data, we do not incorporate this complexity at this stage of the modeling. Instead, we first study the behavior of three coupled point-oscillators in which each oscillator is modeled using the apical parameters of the full model. We will use different parameters for the apical and basal regions only in the spatially distributed model (Model 2).

In Model 1 the concentration of IP_3 , p , is assumed to rapidly attain the steady-state concentration of $p_{\text{st}}^{(i)}$, where the superscript i takes the values 1,2,3, and refers to each of the three cells in the triplet. The cells are coupled through diffusion of Ca^{2+} with coupling strength, ε (s^{-1}). A detailed description and justification of each of the model components can be found in Sneyd et al. (2003). The system of ordinary differential Eqs. 12–20 corresponding to this model is given in Appendix 1. If each $p_{\text{st}}^{(i)}$ is the same (i.e., $p_{\text{st}}^{(1)} = p_{\text{st}}^{(2)} = p_{\text{st}}^{(3)}$), then the model describes the response of three identical cells, with identical levels of agonist stimulation and thus identical $[\text{IP}_3]$. By varying the levels of stimulation in each individual cell of the cluster, i.e., by

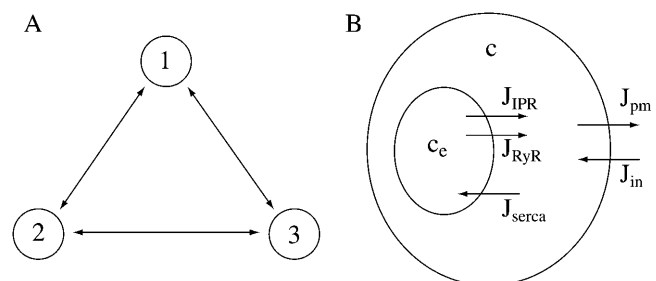


FIGURE 1 (A) Schematic diagram of Model 1, the point-oscillator model. (B) Schematic diagram of the single-cell model.

choosing different values of $p_{st}^{(i)}$ in each cell, we can study synchronization in a group of coupled cells, each with a different intrinsic period.

Numerical method

The model equations (Eqs. 12–20) were solved numerically and the bifurcation analysis was performed using the software package XPPAUT (Ermentrout, 2002), which contains a front-end for AUTO (Doedel et al., 1997).

Results

Steady states

The model of three identical diffusively coupled cells has a symmetric steady state, characterized by identical variable values for all cells. In all the results we discuss here, we use the parameters given in Table 1. The parameters p_{st} and ε are treated as bifurcation parameters. To model a heterogeneous cluster of cells, we assume that p_{st} , which denotes the level of agonist stimulation, is different in different cells. In this case, each model cell has a different resting $[IP_3]$. Because of the complexity of studying multidimensional bifurcation surfaces, the more complicated case, where each cell has different parameter values, is not considered here.

The stability of the symmetric steady state of three interacting cells was analyzed by linearization of the system equations (Eqs. 12–20) in the neighborhood of the symmetric steady state. As shown in Appendix 2, the char-

acteristic polynomial of the eigenvalues λ of the Jacobian may be factorized into two parts, such that

$$F(\lambda) \times D(\lambda)^2 = 0. \quad (1)$$

The factor $F(\lambda)$ corresponds to the characteristic polynomial of the single cell, and is therefore of ninth degree, because of Eqs. 12–20. The other factor, $D(\lambda)$, is of ninth degree as well. The possibility of such a factorization was also demonstrated in systems describing glycolytic oscillations in yeast cells (Wolf and Heinrich, 1997). The solutions of Eq. 1 determine the stability of the steady state.

Dynamics of a single cell

The Ca^{2+} dynamics of an isolated pancreatic acinar cell have been well studied experimentally. It has been observed that physiological doses of cholecystokinin induce baseline spikes of Ca^{2+} , whereas acetylcholine produces faster, sinusoidal, oscillations (Cancela et al., 2002; Cancela, 2001; Lawrie et al., 1993; Yule et al., 1991). Like many other cell types exhibiting IP_3 -induced Ca^{2+} oscillations (Berridge and Dupont, 1994) there exists a critical agonist dose above which a pancreatic acinar cell responds with Ca^{2+} oscillations. In addition, the period of the oscillations decreases with increasing agonist stimulation.

In the case of a single cell, Model 1 reproduces these experimental observations. The dynamics of a single cell as p_{st} varies is summarized in Fig. 2 A. The steady state is stable for small and large values of p_{st} , and there is an intermediate region of values between the two Hopf bifurcation points (HB_1 and HB_2), where the steady state loses stability. The bifurcation at HB_2 is supercritical, i.e., it gives rise to a stable branch of periodic solutions and, as p_{st} decreases, this branch loses stability in a neighborhood of HB_1 . The Hopf bifurcation HB_1 is supercritical as well but the branch that originates from HB_1 has no physiological significance. The behavior of our system in a neighborhood of HB_1 is very complex and beyond the scope of this study. Therefore it is omitted in Fig. 2 A and the bifurcation diagram is not complete. However, the branch that originates from HB_2 corresponds to stable oscillations in $[Ca^{2+}]$ with physiological period and amplitude. Moreover the period of the oscillations increases as p_{st} , and hence the agonist dose, decreases.

Dynamics of three coupled cells

The dynamics of three coupled oscillators has been studied in detail in a number of publications (Ashwin et al., 1990; Baesens et al., 1991; Takamatsu et al., 2001; Yoshimoto et al., 1993). Ashwin et al. (1990), in particular, studied three identical oscillators with weak symmetric coupling, whereas Baesens et al. (1991) performed a detailed study of three non-identical (i.e., with three different intrinsic frequencies) weakly coupled oscillators. In contrast, Takamatsu et al. (2001) and Yoshimoto et al. (1993) investigated specifically

TABLE 1 The parameter values are those used in Sneyd et al. (2003), and are discussed in detail therein

Type of parameter			
Structural			
k_f (apical)	0.71 s ⁻¹	k_f (basal)	0.32 s ⁻¹
v_1 (apical)	0.098 s ⁻¹	v_1 (basal)	0.04 s ⁻¹
v_1 (buffer)	0.08 s ⁻¹	V_{mito} (buffer)	100 s ⁻¹
Transport			
γ	5.405	δ	0.1
J_{er}	0.002 s ⁻¹	α_1	0.2 μM s ⁻¹
V_{serca}	120 μM s ⁻¹	α_2	0.05 s ⁻¹
K_{serca}	0.18 μM	D_c	20 (μm) ² s ⁻¹
V_{pm}	28 μM s ⁻¹	D_p	300 (μm) ² s ⁻¹
K_{pm}	0.425 μM	β	0.8 s ⁻¹
IPR			
k_1	0.64 s ⁻¹ (μM) ⁻¹	k_{-4}	0.54 s ⁻¹
k_{-1}	0.04 s ⁻¹	L_1	0.12 μM
k_2	37.4 s ⁻¹ (μM) ⁻¹	L_3	0.025 μM
k_{-2}	1.4 s ⁻¹	L_5	57.4 μM
k_3	0.11 s ⁻¹ (μM) ⁻¹	l_2	1.7 s ⁻¹
k_{-3}	29.8 s ⁻¹	l_4	1.7 (μM) ⁻¹ s ⁻¹
k_4	4 s ⁻¹ (μM) ⁻¹	l_6	4707 s ⁻¹
RyR			
k_a^+	1500 s ⁻¹ (μM) ⁴	k_a^-	28.8 s ⁻¹
k_b^+	1500 s ⁻¹ (μM) ³	k_b^-	385.9 s ⁻¹
k_c^+	1.75 s ⁻¹	k_c^-	0.1 s ⁻¹

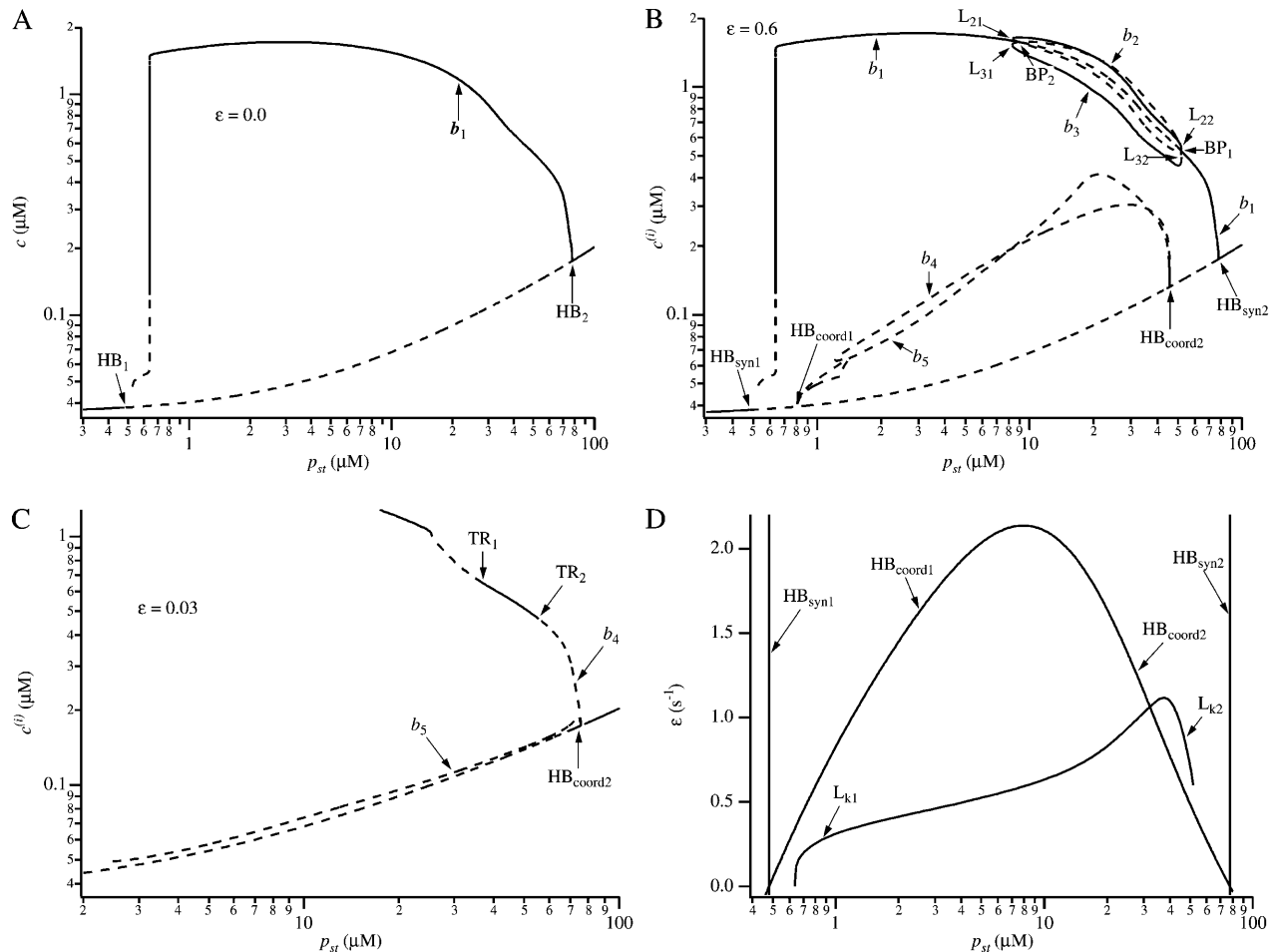


FIGURE 2 (A) Bifurcation diagram of the single-cell model, showing the maximum of the periodic orbits as a function of p_{st} . (B) Bifurcation diagram of Model 1 for $\epsilon = 0.6$, showing the maximum of the periodic orbits as a function of p_{st} . (C) Magnified view of branches b_4 and b_5 for $\epsilon = 0.03$. (D) Two-parameter bifurcation diagram in (p_{st}, ϵ) -space. (HB , Hopf bifurcation; BP , branch point; L , saddle node of periodic; TR , Torus bifurcation point.) The broken lines denote instability. In these computations, as in all other computations on Model 1, we use the apical parameter values.

designed experimental systems of three coupled oscillators. Although most of the various modes of collective behavior found theoretically, as well as observed experimentally, are predicted by symmetric bifurcation theory (Golubitsky and Stewart, 2002), this theory does not apply when the differences between the oscillators are large.

Thus, as pointed out in Strogatz and Stewart (1993), the possible types of collective behavior in a system of three diffusively and all-to-all coupled oscillators (in the case of three cells all-to-all and nearest-neighbor coupling schemes coincide) could be classified according to the strength of coupling and the relative differences between the individual oscillators in the following way:

1. In the limit as the coupling strength goes to zero, each of the oscillators follows its own dynamics and behaves independently. This case corresponds to asynchronous oscillations.
2. In the case of weak coupling, if the three oscillators are identical, then complex behavior, including synchronous

and symmetric and asymmetric phase-locked oscillations, is feasible and depends on the symmetry properties of the whole dynamical system. If the differences among the coupled oscillators are significant, then the common frequency of the phase-locked oscillations is determined by the fastest oscillator.

3. In the case of strong coupling (in which case only synchronized collective behavior is observed) there are two major possibilities: First, if the three oscillators are identical (or the differences between them are negligible), then all of them behave as one, i.e., the dynamics of the whole system could be approximated with the dynamics of an individual oscillator. Second, if the differences among the coupled oscillators are significant, then the common frequency of the synchronized oscillations is approximately just below the average of the intrinsic periods of each individual oscillator; and when the differences between the oscillators are big and the coupling is strong, the phenomenon of oscillator death may take place.

Homogeneous cluster of three cells

The homogeneous cluster of three cells can be regarded as a $D_3(S_3)$ symmetric bi-directional ring of three identical nonlinear oscillators with identical, diffusive two-way nearest-neighbor coupling (Fig. 1 A). According to the theory of symmetry-breaking bifurcations (Golubitsky and Stewart, 2002), there are several oscillatory branches, each corresponding to a different isotropy subgroup of $D_3 \times S^1$. In other words, there are a number of possible oscillatory modes, predicted by the equivariant Hopf bifurcation theory, in which a bi-directional ring of three cells could synchronize.

To study a homogeneous cluster of three cells we assume that $p_{st}^{(i)} = p_{st}$ is the same for each cell. Our point-oscillator model then exhibits most of the predicted oscillatory behaviors. Fig. 2 B presents the bifurcation diagram of three identical coupled cells for a fixed value of $\varepsilon = 0.6$ (s^{-1}) by using p_{st} as the bifurcation parameter. This scheme is valid for all three variables $c^{(i)}$, $i = 1, 2, 3$ since the type of the dynamical behavior, i.e., whether it is a steady-state or oscillatory state, is the same for all variables for any given values of p_{st} and ε , due to the D_3 -symmetry properties of the system.

Fig. 2 B clearly demonstrates that the dynamics of three coupled cells is much more complex than that of a single cell. The steady state in Fig. 2 B loses stability inside a region of p_{st} values, bounded by the pair of Hopf bifurcation points, HB_{syn1} and HB_{syn2} . Note that, because the coupled oscillators are identical, $p_{st}(HB_{syn1})$ and $p_{st}(HB_{syn2})$ have the same values as in the case of a single cell (as shown in Fig. 2 A, where they are labeled HB_1 and HB_2). In the three-cell model a second pair of Hopf bifurcation points, HB_{coord1} and HB_{coord2} , result from the factor $D(\lambda)$. These new Hopf bifurcations occur on the unstable branch of the symmetric steady state.

Branch b_1 (Fig. 2 B), originating from the rightmost Hopf bifurcation point, HB_{syn2} , loses its stability for a range of p_{st} values bounded by a pair of symmetry breaking bifurcation points, BP_1 and BP_2 . On b_1 all three cells oscillate with identical amplitudes and in synchrony (phase shift $\tau = 0$ between the cells). The symmetry breaking bifurcation points, BP_1 and BP_2 , give rise to two more branches, b_2 and b_3 , which have stable and unstable parts and connect the points BP_1 and BP_2 . Both branches b_2 and b_3 originate via subcritical bifurcations and become stable through saddle-

node-of-periodics bifurcations for a region of p_{st} values between L_{21} and L_{22} , and L_{31} and L_{32} , respectively. Because of the D_1 -symmetry we have $p_{st}(L_{21}) = p_{st}(L_{31})$ and $p_{st}(L_{22}) = p_{st}(L_{32})$. Those branches correspond to asymmetric phase-locked oscillations, when two of the cells oscillate in phase and the third cell oscillates out of phase with the other two cells (with phase shift $0 < \tau < T/3$) and slightly different amplitudes determined by b_2 and b_3 (for an example, see Fig. 3 A). The range of p_{st} values where this type of collective behavior exists becomes smaller as the coupling strength, ε , increases, and is replaced by stable synchronous oscillations. The bifurcation diagram of the whole system for values of $\varepsilon > 2.133$ (s^{-1}) looks exactly like the bifurcation diagram of a single cell ($\varepsilon = 0$). We discuss this further below.

There are two more branches, b_4 and b_5 (Fig. 2, B and C), originating from HB_{coord2} . When the coupling strength, ε , is small, branch b_4 becomes stable via a Torus bifurcation, for a range of p_{st} values bounded by TR_1 and TR_2 (Fig. 2 C), and corresponds to symmetric phase-locked oscillations with phase shift $\tau = T/3$ between each pair of cells and identical amplitudes (for an example, see Fig. 3 B). As ε increases, branch b_4 loses stability, whereas branch b_5 is found to be unstable for all values of p_{st} and ε .

The main bifurcations HB_{synj} , HB_{coordj} , and L_{kj} ($j = 1, 2$ and $k = 2, 3$) explained above are shown in Fig. 2 D, where, in addition to p_{st} , the parameter ε is varied. These two-parameter continuations divide the (p_{st}, ε) plane into different regions corresponding to different dynamical behaviors. In the regions left of the line HB_{syn1} and right of the line HB_{syn2} , the system will always approach a stable steady state. Between the lines HB_{synj} ($j = 1, 2$) the steady state is unstable and the system will tend toward one of the limit cycles representing synchronous, phase-locked, or asynchronous oscillations. In Fig. 2 D the lines L_{kj} ($j = 1, 2$ and $k = 2, 3$) are represented by a single line because $p_{st}(L_{21}) = p_{st}(L_{31})$ and $p_{st}(L_{22}) = p_{st}(L_{32})$ for all values of ε . Above the line, L_{kj} -only stable synchronous oscillations are possible, whereas below HB_{coordj} and L_{kj} ($j = 1, 2$ and $k = 2, 3$), stable asymmetric phase-locked, and stable or unstable (depending on the value of ε) symmetric phase-locked oscillations, may exist.

Fig. 2, B–D, reveals that there are parameter regions where different stable oscillatory modes may coexist,

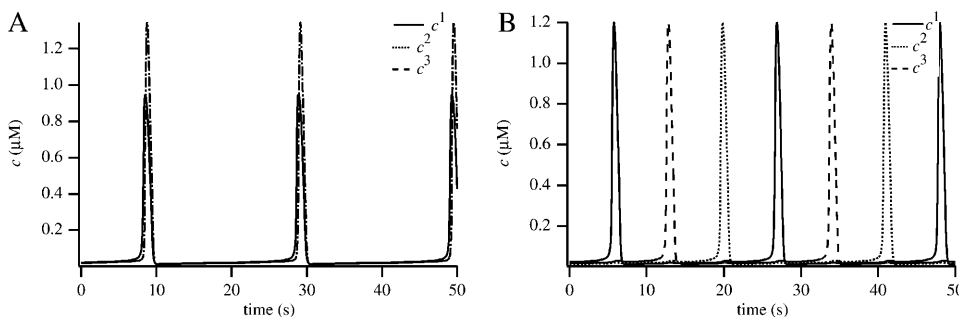


FIGURE 3 (A) Typical asymmetric phase-locked oscillations in Model 1 for $\varepsilon = 0.6$ and $p_{st} = 20.6$. (B) Typical symmetric phase-locked oscillations in Model 1 for $\varepsilon = 0.03$ and $p_{st} = 20$.

depending on the initial conditions. The simultaneous occurrence of stable portions of branches b_1 , b_2 , and b_3 in a neighborhood of the bifurcation points BP_1 and BP_2 , or stable parts of branches b_2 , b_3 , and b_4 at low values of ε , accounts for bi-rhythmicity in the present model. Moreover, for very small regions of p_{st} and ε -values, the coexistence of stable portions of branches b_1 , b_2 , b_3 , and b_4 indicates that there exists even a tri-rhythmicity of asynchronous oscillations and two kinds of phase-locked behavior—symmetric and asymmetric.

Heterogeneous cluster of three cells

Real cells are not identical. For instance, there is experimental evidence that different pancreatic acinar cells respond differently to the same level of agonist stimulation (Ngezahayo and Kolb, 1993). When differences between the cells are small, i.e., they oscillate with similar frequencies, the results from the analysis of the homogeneous cluster of three cells will be a good approximation for the collective behavior of a heterogeneous cluster. However, this is not the case when those differences are larger.

To investigate the situation when the differences among the individual cells are significant, we study Model 1 using different values for $p_{st}^{(i)}$, $i = 1, 2, 3$ for each individual cell. Since each cell will thus have a different intrinsic frequency, to respond in synchrony the frequencies of the different cells in the cluster must adjust to those of their neighbors. Our analysis shows that this can be accomplished by gap-junctional diffusion of Ca^{2+} . For that purpose, we study Model 1 again, using p_{st} and ε as the main bifurcation parameters.

Of course, there are many other ways in which the cluster of cells could be made heterogeneous. Varying any of the parameters from cell to cell would accomplish the task. However, the ultimate effect of such changes is effectively expressed in the intrinsic frequency of the cells. No matter how the intrinsic frequency is changed, the qualitative effect will be the same. Thus for our purposes it is sufficient merely to vary $p_{st}^{(i)}$ to obtain these different intrinsic frequencies.

In the heterogeneous case, the steady state generally has three pairs of Hopf bifurcations (Fig. 4 A), arising when pairs of eigenvalues cross the imaginary axis. As in the single cell, the steady state is stable for small and large values of p_{st} , and

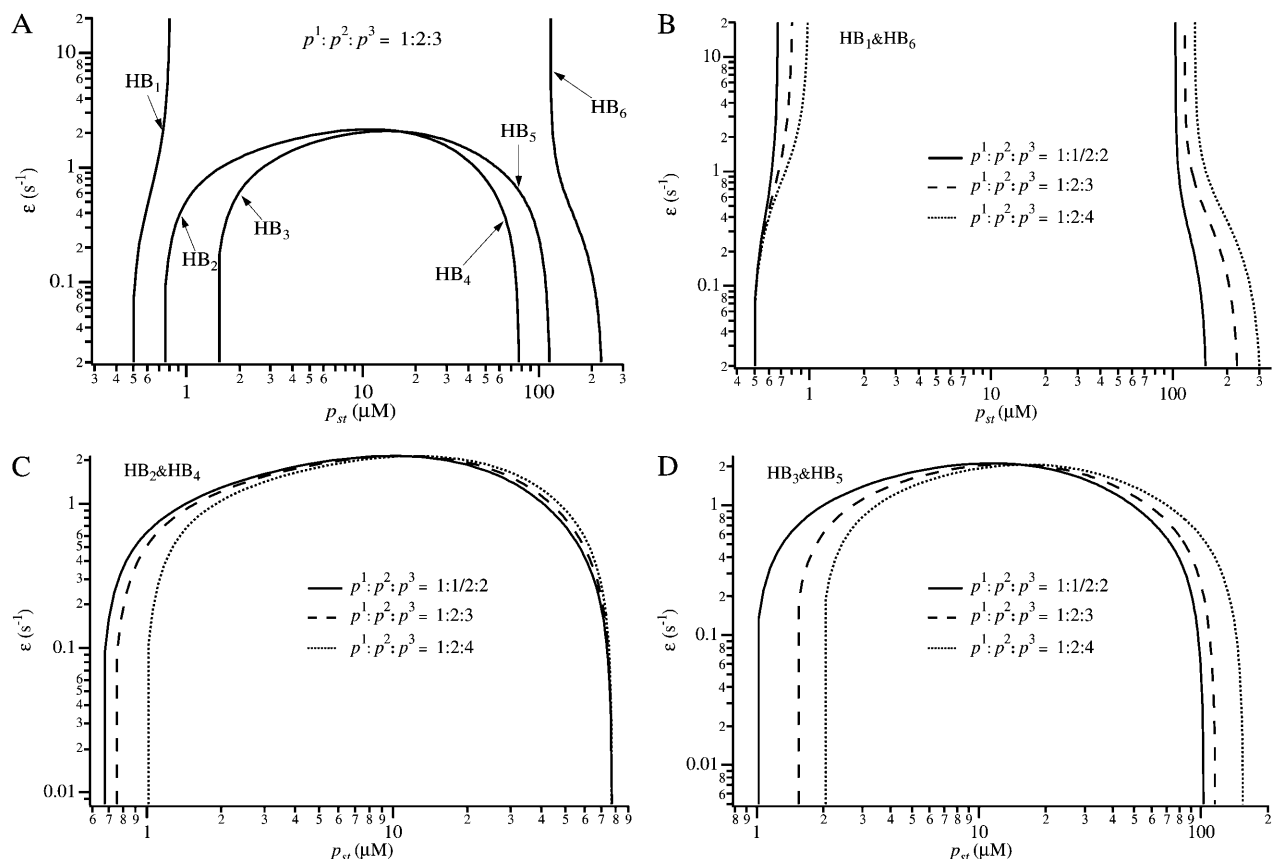


FIGURE 4 Two-parameter bifurcation diagram in (p_{st}, ε) -space. (A) Loci of the Hopf bifurcation points of Model 1 in the case of a heterogeneous cluster of three cells. (B) Locus of the first pair of Hopf bifurcation points of Model 1 for triplets of cells with varying degrees of heterogeneity. (C) Locus of the second pair of Hopf bifurcation points of Model 1 for triplets of cells with varying degrees of heterogeneity. (D) Locus of the third pair of Hopf bifurcation points of Model 1 for triplets of cells with varying degrees of heterogeneity.

in the intermediate region between the Hopf bifurcation points, HB_1 and HB_6 (which arise when the first pair of eigenvalues crosses the imaginary axis), it loses stability. There are two more pairs of Hopf bifurcation points, HB_2 and HB_4 , and, HB_3 and HB_5 , originating respectively from the second and the third pair eigenvalues. The system (Eqs. 12–20) exhibits oscillatory behavior between HB_1 and HB_6 . Fig. 4 summarizes the loci of the Hopf bifurcation points existing in the system for three different degrees of heterogeneity ($p_{st}^1:p_{st}^2:p_{st}^3 = 1:1.5:2$, $p_{st}^1:p_{st}^2:p_{st}^3 = 1:2:3$, and $p_{st}^1:p_{st}^2:p_{st}^3 = 1:2:4$) in the p_{st} - ε -plane.

As the degree of heterogeneity increases, the range of values of p_{st} where oscillations are found increases. It is easily seen why this is so. Although a particular cell might not oscillate when in isolation, it can be driven to do so by its neighbors. The greater the spread of intrinsic frequencies, the more this will happen (assuming the cells are coupled strongly enough), and thus oscillations over the whole cluster will appear for a wider range of stimulus strengths.

If the cells are uncoupled, i.e., there is no gap-junctional diffusion of Ca^{2+} , each cell oscillates with its intrinsic frequency (Fig. 5, A and C, and Fig. 6, A and C). Similar asynchronous behavior is observed for non-zero but very small ($\varepsilon \approx 0$) coupling. When the coupling is weak (for our system, $\varepsilon < 0.8$ (s^{-1})) there are several possible stable oscillations. The branch originating at HB_4 appears to be unstable for all values of p_{st} and ε . In the case of weak coupling the branch arising from HB_5 , initially unstable, becomes stable via a Torus bifurcation and gives phase-locked (1:1:1) behavior with the common period determined by the fastest cell in the cluster, as shown in Fig. 5, A and B. Such increases in the frequency of a coupled triplet of pancreatic acinar cells compared to the single cell have been reported in Petersen and Petersen (1991). Furthermore, period-doubling bifurcations on the same branch (originating at HB_5) give rise to phase-locked behavior different from

(1:1:1). Fig. 5 D illustrates an example of such a behavior, with ratios (1:2:2), i.e., where the slowest oscillator drops out of every other cycle. When the coupling strength is small the branch originating from HB_6 is stable only for very large values of p_{st} and loses stability via a Torus bifurcation approximately at $p_{st}(HB_5)$.

Increasing the degree of coupling still further leaves us with a single stable branch of periodics, namely the branch that originates at HB_6 . This branch corresponds to synchronized behavior with averaged period and amplitude (Fig. 6, B and D). The degree of averaging depends on the coupling strength as well as on the level of stimulation, p_{st} , i.e., the greater the coupling or the level of stimulation, the closer are the phases and the amplitudes of the cells in the cluster. These results agree very well with the experimental conclusions of Stauffer et al. (1993), who showed that increasing gap-junctional permeability with NO_2^- synchronizes the amplitude and frequency of the cholecystokinin evoked $[Ca^{2+}]_i$ oscillations.

MODEL 2: SPATIALLY DISTRIBUTED CELLS

We now study the behavior of a model in which each cell can exhibit spatial gradients of Ca^{2+} and IP_3 . Since the model is now spatially distributed this allows us to let different regions of the cells have different parameter values, and thus model the polarized nature of a pancreatic acinar cell (Ashby et al., 2002; Fogarty et al., 2000a; Kasai et al., 1993). Our initial numerical simulations of Model 2 will not be so complex, however, but will instead just assume that each cell has the same parameters throughout (parameters corresponding to the apical region). We call such cells *homogeneous*. This initial simplified approach will facilitate comparison with the results of Model 1, for which we used the apical parameters. However, we will then discuss simulations of the

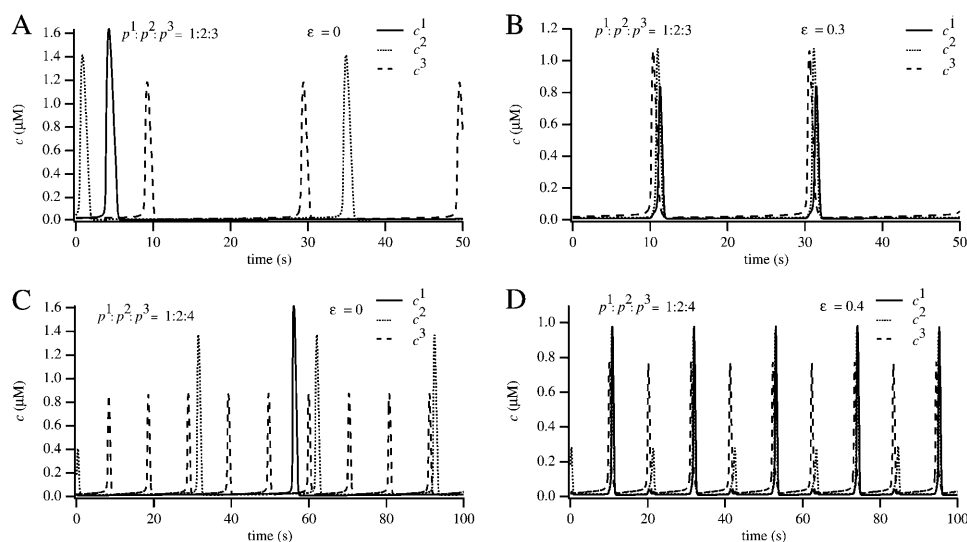


FIGURE 5 Typical oscillations in Model 1 in the case of weak coupling. A and B correspond to mild heterogeneity, and C and D to greater heterogeneity. (A) Uncoupled cells; (B) typical asymmetric phase-locked oscillations in Model 1 with weak coupling. Here, the common frequency is determined by the fastest cell in the cluster. These oscillations arise via a Torus bifurcation when the branch of periodic orbits originating at HB_5 gains stability. (C) Uncoupled cells; (D) typical phase-locked (1:2:2) oscillations in Model 1 with weak coupling. These oscillations correspond to a branch of periodic orbits arising via a period doubling bifurcation on the branch originating at HB_5 .

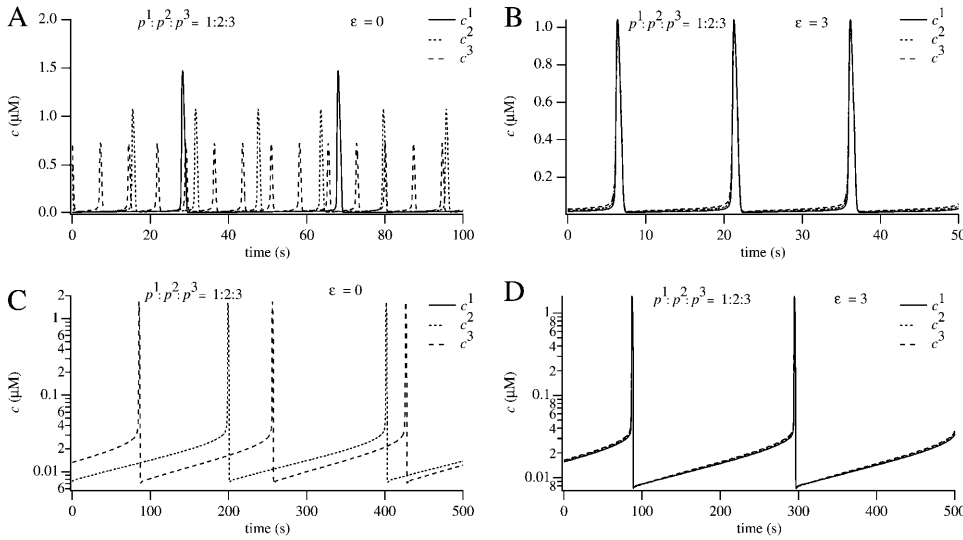


FIGURE 6 Comparison between the typical oscillations in Model 1 at near-threshold (*C* and *D*) level of stimulation and at higher (*A* and *B*) stimulation level. (*A* and *C*) Uncoupled cells. (*B* and *D*) Strongly coupled cells, showing synchronized oscillations. Here the common frequency and amplitude are an average of those of the individual cells. These oscillations correspond to the branch of periodic orbits corresponding to the pair of Hopf bifurcation points HB_1 and HB_6 in Fig. 4 *B*. *A* and *B* use $p^1_{st} = 12.113$, $p^2_{st} = 24.226$, and $p^3_{st} = 36.34$. *C* and *D* use $p^1_{st} = 0.4833$, $p^2_{st} = 0.967$, and $p^3_{st} = 1.45$. Note that in *C* and *D*, *c* is plotted on a log scale.

full model, in which each cell has distinct apical and basal regions. These model cells we call *heterogeneous*.

Description of the model

As before, we use the model of Sneyd et al. (2003), who assumed that the apical and basal regions of the cells have different densities of IP_3 receptors (IPRs) and ryanodine receptors (RyRs), and are separated by a mitochondrial buffer band (Tinel et al., 1999; Straub et al., 2000) (Fig. 7 *C*). The parameter k_f controls the density of IPR, and v_1 controls the density of RyR. The parameter values are determined by fitting to experimental data (Sneyd et al., 2003). Both Ca^{2+} and IP_3 are assumed to diffuse, with constant diffusion coefficients of D_c and D_p , respectively. We do not include explicit buffers, and hence all the diffusion coefficients, as well as all the Ca^{2+} fluxes, are defined as effective diffusion coefficients and fluxes.

Within each cell, the concentration of IP_3 is assumed to tend toward the steady state of $p^{(i)}_{st}$, $i = 1, 2, 3$ with a time constant of $1/\beta$ s. As before, we model agonist stimulation by an increase in $p^{(i)}_{st}$. $[IP_3]$, denoted by p , then obeys the reaction-diffusion equation

$$\frac{\partial p^{(i)}}{\partial t} = D_p \nabla^2 p^{(i)} + \beta(p^{(i)}_{st} - p^{(i)}). \quad (2)$$

$p^{(i)}_{st}$ is assumed to be spatially homogeneous within each cell, i.e., each part of the cell tends toward the same $[IP_3]$ after agonist stimulation. However, it is important to note that, although within each cell p_{st} is not spatially varying, nevertheless the steady-state distribution of IP_3 will *not* be spatially homogeneous within each cell. Because each cell has a different value of p_{st} , intercellular diffusion of IP_3 will cause steady-state spatial gradients of IP_3 , particularly close to the intercellular boundaries.

The same is true of the resting distribution of Ca^{2+} . Due to the asymmetric geometry of the acinus, and the fact that each cell has different apical and basal regions, spatial Ca^{2+} gradients will be introduced at rest. Thus the steady state must be found numerically, by starting with reasonable, random, initial conditions, and integrating until the steady state is reached. All the simulations of Model 2 use this spatially heterogeneous steady state as the initial condition.

The two-dimensional version of the model consists of two reaction-diffusion equations, Eqs. 28 and 29, describing the reaction and diffusion of cytosolic Ca^{2+} and IP_3 respectively, coupled to a system of seven ordinary differential equations, Eqs. 13–19, for the dynamics of the Ca^{2+} concentration in the ER, the IPR, and the RyR. A summary of the model equations is given in Appendix 1, and the parameter values are given in Table 1.

Incorporation of gap junctions

Gap junctions in pancreatic acinar cells are permeable to both Ca^{2+} and IP_3 and allow the diffusion of diverse small-sized molecules between neighboring cells (Ngezahayo and Kolb, 1993; Petersen and Petersen, 1991; Stauffer et al., 1993; Yule et al., (1996). Therefore we incorporate gap-junctional diffusion of both molecules in our model. We assume that at each internal cell boundary the flux is dependent on the concentration difference across the membrane as well as on the permeability of the gap junctions to Ca^{2+} and IP_3 , respectively. Thus, at each intercellular boundary

$$-D_c \nabla c^- \cdot n = -D_c \nabla c^+ \cdot n = c_f(c^- - c^+), \quad (3)$$

and

$$-D_p \nabla p^- \cdot n = -D_p \nabla p^+ \cdot n = p_f(p^- - p^+), \quad (4)$$

where n is the outward-pointing unit normal and the superscripts $+$ and $-$ denote the Ca^{2+} and IP_3 concentrations

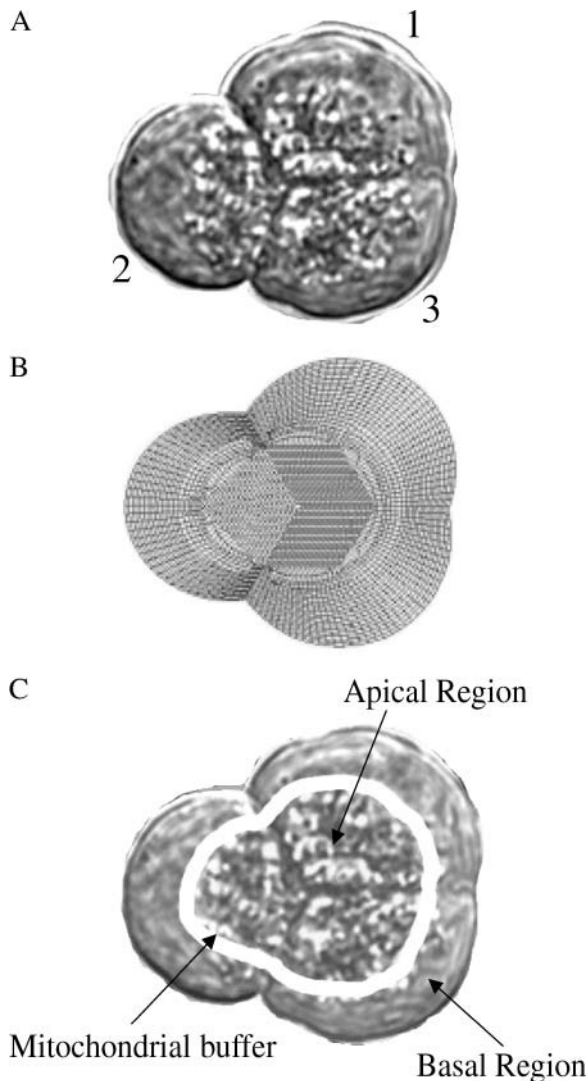


FIGURE 7 (A) Experimental image of a cluster of three pancreatic acinar cells; (B) the mesh upon which we solve the equations of Model 2 using a finite element method. (C) Experimental image of the cluster showing the approximate positions of the apical and basal regions that were used in the model.

at the right and left limits of the border, respectively. The junctional permeability coefficients, with units of distance/time ($\mu\text{m s}^{-1}$), c_f to Ca^{2+} and p_f to IP_3 , are unknown parameters whose values are chosen to give reasonable agreement with experimental observations.

Numerical method

The model equations (Eqs. 28 and 29) were solved using a standard Galerkin Finite Element method and the rest of the model equations were solved by a backward Euler method in two spatial dimensions on a finite element mesh (Fig. 7 B) based on a real image of a triplet of pancreatic acinar cells (Fig. 7 A). No-flux boundary conditions were applied on the

external borders of each cell and the cells were connected by the internal boundary conditions, Eqs. 3 and 4. Explicit gap junctions were not included in the numerical simulations; it was assumed that IP_3 and Ca^{2+} can diffuse between cells at any grid point on the internal borders. The equations were solved on a mesh with 1301 grid points (nodes) corresponding to 1239 elements within each cell. The location of the apical, the mitochondria buffer, and the basal regions were approximately determined by comparing to the experimental images for each of the cells (Fig. 7 C).

Results

Dynamics of a single cell

The dynamics of a single spatially distributed cell is discussed in detail in Sneyd et al. (2003). For completeness we will outline here some of the main results from this analysis. Due to the lower receptor densities, the basal responses are smaller than in the apical region, which agrees well with experimental data (Kasai et al., 1993; Straub et al., 2000). Furthermore, model simulations show that Ca^{2+} rises in the apical region first, followed by a wave-spread across the basal region as has been experimentally observed (Fogarty et al., 2000b; Kasai et al., 1993; Lawrie et al., 1993; Leite et al., 2002; Nathanson et al., 1992; Straub et al., 2000; Thorn et al., 1993; Thorn, 1996). At low agonist stimulation mitochondrial uptake can eliminate an intracellular Ca^{2+} wave, but only does so for a narrow range of parameter values. This is consistent with the relatively narrow range of IP_3 concentrations in which Ca^{2+} signals confined to the apical region in pancreatic acinar cells have been observed (Straub et al., 2000). The model predicts that there are two distinct mechanisms of wave propagation. At low $[\text{IP}_3]$ the Ca^{2+} wave is transmitted from the apical to the basal region by an active wave, dependent on diffusion of Ca^{2+} between release sites, whereas at high $[\text{IP}_3]$ the intracellular phase waves result from differences in the intrinsic frequencies of the oscillations in the apical and basal regions. In this second case, the wave is called a *kinematic wave*, and does not depend on Ca^{2+} diffusion.

Dynamics of three coupled cells

When the cells are identical each cell eventually ends up with the same $[\text{IP}_3]$ and thus the diffusion of IP_3 through gap junctions has no influence on the long-term collective behavior of the cluster. However, by assuming that each cell has a different value of $p_{\text{st}}^{(i)}$, we are able to generate intercellular $[\text{IP}_3]$ gradients. This is consistent with the suggestion made in Yule et al. (1996) that differences in the intrinsic frequencies of oscillations among the cells in a triplet are most likely due to differences in the ability of different cells to produce IP_3 . Such differences have also been identified as gradients in agonist sensitivity, which implies differences in $[\text{IP}_3]$ between connected cells.

We are interested in whether the results from the analysis of the point-oscillator model, where we have used apical parameter values, could be related to the results from the analysis of the spatially distributed model. Therefore we begin by neglecting the spatial heterogeneity inside each cell and use only apical parameter values over the three cells. In this way the cells differ in size and shape, and are spatially distributed, but have the same parameters throughout. Later we include the structural heterogeneity of each cell by assuming different parameters in the apical and basal regions.

Homogeneous cells; only apical parameter values

First we study the simpler case where either Ca^{2+} or IP_3 gap-junctional flux is assumed to be zero, i.e., the cells in the cluster are assumed to communicate only through one of the two possible messengers. Intercellular diffusion of IP_3 alone fails to coordinate Ca^{2+} oscillations even for unrealistically large values of IP_3 permeability (computations not shown). In contrast, setting $p_f = 0$ ($\mu\text{m s}^{-1}$), i.e., preventing IP_3 diffusion between cells, does not prevent the long-term development of synchronized oscillations (computations not shown). We conclude that Ca^{2+} is necessary and sufficient for synchronizing Ca^{2+} oscillations. However, it has been experimentally verified (Ngezahayo and Kolb, 1993; Petersen and Petersen, 1991; Stauffer et al., 1993; Yule et al., 1996) that IP_3 also diffuses through gap junctions. So, if the junctional flux of IP_3 is not the reason for the long-term spatial organization of Ca^{2+} signals in coupled cells, then does it contribute in this process and, if so, to what extent?

We suggest that IP_3 gap-junctional diffusion contributes to synchronization of Ca^{2+} oscillations in connected cells by decreasing the differences in the individual oscillators' periods. Hence smaller amounts of Ca^{2+} diffusing through gap junctions (represented by smaller values of c_f) will be enough to coordinate the oscillations in $[\text{Ca}^{2+}]$. (By coordinated behavior we mean either synchronous or phase-locked.) This is illustrated in Fig. 8, where the respective regions of phase-locking and synchronization in the two parameter space (p_f, c_f) are outlined. It is clearly seen that increasing IP_3 permeability leads to a decrease in the value of c_f which is sufficient to coordinate the three cells in the cluster. It is worthwhile to note that qualitatively the same result follows from similar simulations with the point-oscillator model in which IP_3 as well as Ca^{2+} is allowed to diffuse (computations not shown).

There are some interesting differences between the behavior of the point-oscillator and spatially distributed models. As can be seen in Fig. 2, B–D, the point-oscillator model can exhibit both symmetric and asymmetric phase-locked oscillations; in numerical simulations the type of oscillation that develops depends on the initial conditions. This is not the case in the spatially distributed model. In Fig. 9 A we show that even when the initial condition is the

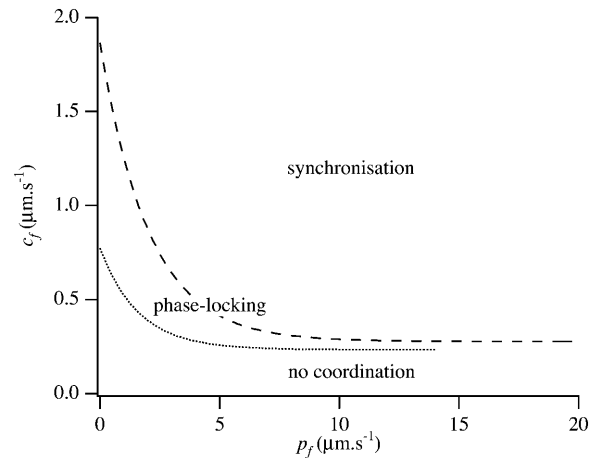


FIGURE 8 Two-parameter diagram in (p_f, c_f)-space showing approximate regions where synchronous, asynchronous, and phase-locked behavior occurs. Using the parameters $p_1 = 10$, $p_2 = 20$, and $p_3 = 30$, we solved the model equations until approximate steady-state behavior was obtained. Since effects of hysteresis were not investigated, and due to limited resolution in p_f and c_f , the boundaries are only approximate.

symmetric phase-locked mode, it is unstable and only persists for a short time before spontaneously switching to asymmetric phase-locked oscillations. It appears that the symmetric phase-locked oscillation is destabilized by the asymmetric geometry of the acinus. Another interesting effect of the geometry of the cells can be found in the different ways in which the traces taken from the apical and basal part of the cells coordinate (Fig. 9, A and B). Note that, since the cells are homogeneous (i.e., with no difference between the apical and basal parameters), any differences in the responses must be due to geometrical effects. The apical regions become phase-locked, and the apical response in each cell oscillates with a similar amplitude. However, the basal traces are taken from regions where, due to the geometry of the triplet, the impact of the gap-junctional fluxes is smaller, and thus the phase-locked oscillations show much greater differences in amplitude between the cells. Since secretion occurs from the apical regions it follows that, even in situations where neighboring cells do not have synchronized basal regions, it is still possible to have synchronized multicellular secretion resulting from synchronization of the apical regions.

Heterogeneous cells; apical and basal parameter values

Finally, we discuss the most complicated case in which each cell is spatially distributed, with different parameter values in the apical and basal regions. Most of these simulations have shown a tendency toward the asymmetric phase-locked mode (an example is shown in Fig. 10 A). Preliminary experimental observations indicate that asymmetric phase-locked oscillations are more commonly seen than symmetric ones (see, for instance, Fig. 2 B in Yule et al., 1996). This happens not only in the case of triplets of cells but also in bigger

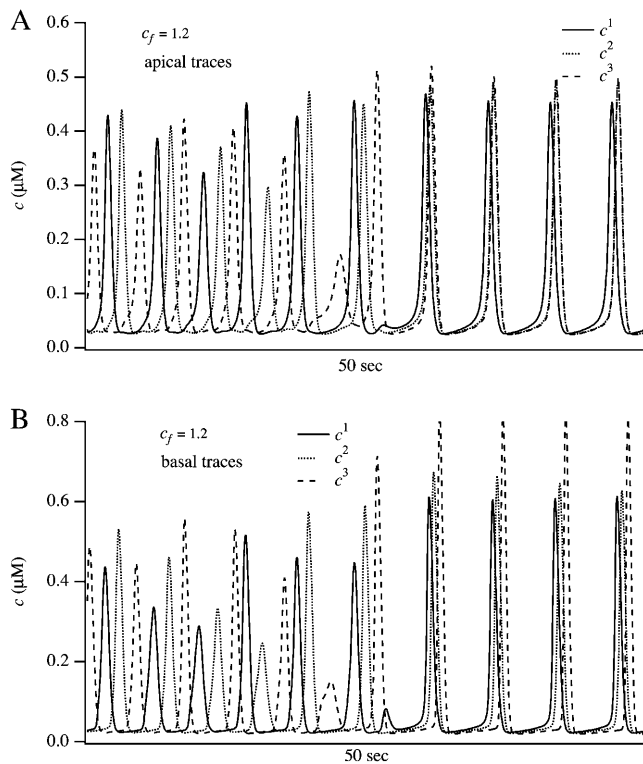


FIGURE 9 Intercellular oscillations in the triplet where each cell is assumed to be homogeneous, i.e., the parameters do not vary within each cell and are assumed to be those of the apical region (Table 1). The concentration of IP_3 is constant ($p_{\text{st}} = 40$) over the three cells, and the cells are identical. Ca^{2+} gap-junctional permeability is set to $c_f = 1.2$. (A) Traces taken from the middle of the apical region; (B) traces taken from the middle of the basal region. (Note that the parameter values are the same for each region but the responses are different because of geometrical factors.)

clusters, where a group of cells responds in synchrony followed by another group (unpublished data). However, this model prediction needs to be confirmed by more extensive analysis of data. Comparison of Fig. 10, A and C, demonstrates again the role of IP_3 gap-junctional diffusion in smoothing the differences between the cells in the cluster. Comparing Fig. 10, A and C, we see that for one and the same strength of Ca^{2+} coupling ($c_f = 0.9 \mu\text{m s}^{-1}$) the type of collective behavior depends on the amount of IP_3 diffusing through gap junctions. When the coupling strength for IP_3 is smaller ($p_f = 2.0 \mu\text{m s}^{-1}$) the differences between the cells are larger and hence they fail to phase-lock (1:1:1) (Fig. 10 C). Increasing the coupling strength for IP_3 ($p_f = 3.0 \mu\text{m s}^{-1}$) leads to asymmetric phase locking, as shown in Fig. 10 A. These theoretical results agree very well with the experimental observations (Ngezahayo and Kolb, 1993) that gap-junctional diffusion modulates the collective oscillatory behavior in coupled pancreatic acinar cells.

Traces taken from the basal regions (Fig. 10, B and D) do not follow exactly the behavior of the apical regions but show the same qualitative behavior. The differences are mainly due to the different structure and shape of the basal

region, as well as differences in the receptor densities in the apical and basal regions.

DISCUSSION AND CONCLUSIONS

We have taken a previous model of Ca^{2+} dynamics in a pancreatic acinar cell (Sneyd et al., 2003) and studied the dynamics of three cells coupled in a ring. Such a geometric arrangement corresponds to what is commonly found in experiment. Our goal was to study whether intercellular diffusion of Ca^{2+} could synchronize intercellular waves, and what role intercellular diffusion of IP_3 plays in such synchronization.

To do this, we constructed two qualitatively different models. Model 1 modeled each cell as a point oscillator, with no spatial dependence, an approach that is commonly used in the study of coupled oscillators. Model 2 assumed each cell to be spatially distributed, coupled by Ca^{2+} and/or IP_3 diffusion through gap junctions along each common border. Since this is a more realistic scenario, our goal was to determine whether analysis of the simpler Model 1 could give any insight into the behavior of the more complex Model 2.

Our results can be summarized as follows:

1. Gap-junctional diffusion of Ca^{2+} plays a crucial role in the coordination of Ca^{2+} oscillations in coupled cells. The degree of coordination depends on the amount of Ca^{2+} diffusing through gap junctions as well as on the gradient of $[\text{IP}_3]$.
2. Diffusion of IP_3 through gap junctions facilitates the synchronization of Ca^{2+} oscillations by minimizing the relative differences in $[\text{IP}_3]$ between connected cells.
3. Although symmetric phase-locked oscillations are stable solutions of Model 1, they do not appear to be stable in Model 2. It appears that the asymmetric geometry of a realistic cluster destabilizes symmetric phase-locked oscillations, which develop instead into asymmetric phase-locked oscillations. Thus our model predicts that the asymmetric mode, in which clumps of cells oscillate in synchrony, would be observed more often experimentally. Preliminary experimental investigations confirm this prediction.
4. The increase in the common frequency of oscillations among connected cells compared with a single cell, as well as the observed appearance of oscillations in cells that would not oscillate if not coupled, strongly suggests the presence of pacemaker cell(s) in multiplets of cells.
5. Analysis of the point-oscillator model is insufficient to determine which kinds of oscillations will appear in clusters of cells with realistic geometries. Geometrical factors play a crucial role in destabilizing some oscillatory patterns.

Our simulations show increases in the frequency of the Ca^{2+} oscillations among connected cells compared to the

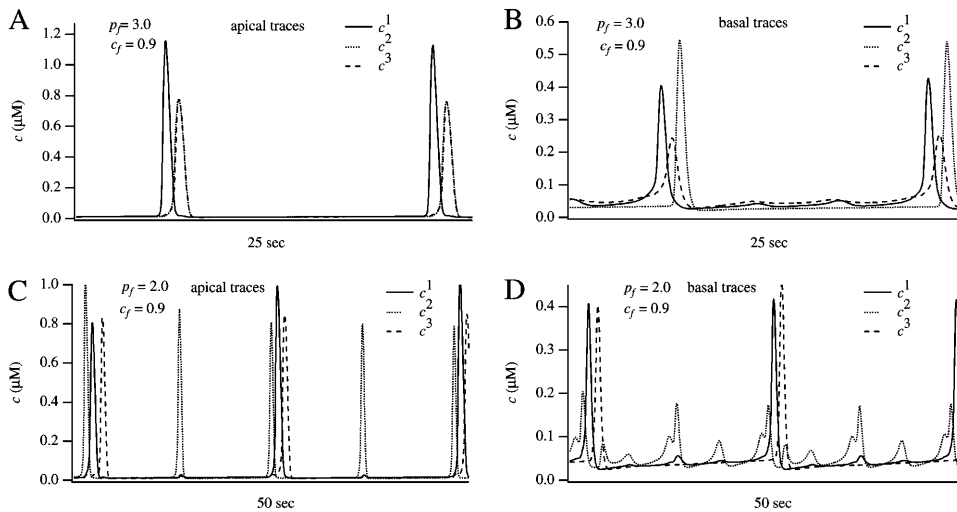


FIGURE 10 Intercellular oscillations in the triplet where each cell is assumed to be heterogeneous, i.e., the apical and basal regions have different parameter values. Traces are taken approximately from the regions denoted by the arrows in Fig. 7 C. Initially $p_{\text{int}} = 17$ over the three cells. In each of the cells the parameter p_{st} is chosen so that the three cells tend to different steady states of $[\text{IP}_3]$ ($p_{\text{st}}^1 = 11$, $p_{\text{st}}^2 = 12$, $p_{\text{st}}^3 = 13$). As the intercellular diffusion of IP_3 increases, phase-locking of the apical regions becomes more pronounced. However, due to their different geometry and size, which results in a lower effective coupling strength, the basal regions show a much lesser degree of coordination.

frequency of a single cell, as has been observed experimentally in small clusters of pancreatic acinar cells (Ngezahayo and Kolb, 1993; Petersen and Petersen, 1991; Stauffer et al., 1993). At moderate levels of Ca^{2+} gap-junctional diffusion the common frequency is determined by the fastest cell in the cluster, as occurs also in coupled hepatocytes (Höfer, 1999). In agreement with the experimental data from pancreatic acinar cells, increasing gap-junctional conductance not only tunes the phase difference of the Ca^{2+} oscillations (Ngezahayo and Kolb, 1993) but also equalizes the amplitude and frequency of these oscillations (Stauffer et al., 1993). Therefore our results are consistent with the presence of a pacemaker cell in coupled multiplets of pancreatic acinar cells, where gap-junctional communication increases their sensitivity range. In this way, as proposed in Yule et al. (1996), the augmentation of a threshold Ca^{2+} response generated in one cell, all over the whole cluster, may result in increased secretion. Such increased enzyme secretion has also been reported in Stauffer et al. (1993).

All of the qualitative results from Model 1 are generic to three coupled oscillators. The various kinds of coupled oscillations predicted by the model are not unique to our particular formulation of the intracellular Ca^{2+} dynamics. Thus any model with the same basic structure (i.e., any model in which Ca^{2+} oscillations occur at constant $[\text{IP}_3]$) would be expected to give the same qualitative results, although, of course, the precise details of the parameter values and the intracellular oscillations would vary. In particular, our conclusions about the crucial importance of gap-junctional Ca^{2+} diffusion for coupling cells would remain unchanged by the use of a different model with the same overall structure. Furthermore, our conclusion that a point-oscillator model is only an indifferent guide to the behavior of a spatially distributed model is independent of the precise model details.

However, there is one aspect of our model that could possibly play an important role in determining multicellular

behavior. A fundamental dynamical feature of our model is that the concentration of IP_3 does not oscillate. Although we have simulated a gradient of $[\text{IP}_3]$ between individual cells, this is not a periodically changing gradient. It is not yet known whether oscillations in $[\text{IP}_3]$ are necessary for Ca^{2+} oscillations in pancreatic acinar cells; experimental evidence so far is inconclusive. If an oscillating $[\text{IP}_3]$ is a crucial feature of this cell type, then this will have an important effect on the predictions from a multicellular model. For instance, if IP_3 oscillations can themselves be synchronized between cells, then it is very likely that gap-junctional diffusion of IP_3 will be sufficient (although perhaps not necessary) for intercellular synchronization. Thus, definitive confirmation of our model predictions awaits first a definitive determination of the role of IP_3 oscillations in the single cell responses.

One other caveat must also be mentioned. In studying the synchronization of multicellular behavior, we have concentrated on the long-time responses, i.e., the kinds of coupled oscillations that develop after many oscillation periods. In the short-term, cells can appear to be synchronized, even though over a longer timescale such synchronization gradually breaks down. This point is very important when comparing model predictions to experimental data. If the data is not collected over a long-enough time period, it is not possible to conclude anything about the long-term synchronization of the cells—in which case, comparison with the model predictions above is problematic.

The values we use for ε (the coupling strength for Ca^{2+} in Model 1) are in the same range as those estimated by Höfer (1999) in a similar study of hepatocytes. In particular, the value of $\varepsilon < 0.8$ (s^{-1}) predicted by our model giving weak coupling between heterogeneous cells, agrees well with the value given in Höfer (1999). Furthermore, the values of p_f (gap-junctional permeability to IP_3) in Model 2, which affect the coordination of Ca^{2+} signal in our analysis, are in very good agreement with the values used in studies of intercellular Ca^{2+} waves in hepatocytes (Dupont et al., 2000b),

astrocytes (Höfer et al., 2002), mixed glial cells (Sneyd et al., 1998), and airway epithelial cells (Sneyd et al., 1995). However, the value of c_f (gap-junctional permeability to Ca^{2+}) predicted by our Model 2, although consistent with the value in Sneyd et al. (1998), is significantly higher than the values estimated in Höfer et al. (2001, 2002). The reason for such a discrepancy may be in the different geometry that we have used as well as in the polarized nature of the pancreatic acinar cells. Unfortunately there are no direct experimental measurements of the Ca^{2+} gap-junctional conductance in pancreatic acinar cells. Therefore the question about the precise values of c_f remains open and requires further experimental and modeling work.

APPENDIX 1: SUMMARY OF THE MODEL EQUATIONS

The model incorporates the dynamics of the cytosolic Ca^{2+} concentration, denoted by c , as well as the dynamics of the Ca^{2+} concentration in the ER, denoted by c_e , and assumes that Ca^{2+} oscillations occur in the presence of a constant IP_3 concentration, denoted by p with steady-state value p_{st} . Fig. 1 *B* illustrates the schematic diagram of the model in the absence of diffusion. Calcium release from the internal store is through both IP_3 receptors (IPRs) and ryanodine receptors (RyRs). An independent constant leak from the internal store, J_{er} , is also included, to balance the action of the ER (SERCA) pump in the absence of any IPR or RyR activity.

The model of the IP_3 receptor that we use is that of Sneyd and Dufour (2002) in which the IP_3 receptor is assumed to exist in one of six states: R , rest state; O , open; S , shut; A , activated; I_1 , first inactivated state; and I_2 , second inactivated state. The derivation of this model is too involved to present in detail here; interested readers are referred to the original article. For the RyR we use the model of Keizer and Levine (1996), in which w denotes the fraction of RyR not in the closed state. Again, the model is too complicated to derive in detail here, and the reader is referred to the original article.

The flux through the receptor is assumed to be proportional to the concentration difference between the ER and the cytoplasm and includes the open probabilities of the IPR and RyR, multiplied by factors k_f and v_1 , respectively, which scale the maximum rate of Ca^{2+} release from ER and are thus indirect measures of the relative densities of IPR and RyR. The Ca^{2+} influx across the plasma membrane, J_{in} , is assumed to depend on the level of agonist stimulation and therefore is represented as a linear increasing function of p . The SERCA ATPase pump is modeled by a hyperbolic dependence on c . In addition a feedback inhibition of Ca^{2+} reuptake, J_{serca} , by c_e is included. Although this model of the SERCA ATPase is not derived from first principles, use of a more realistic Markov state model does not change our results (computations not shown). We assume that the plasma membrane Ca^{2+} pump, J_{pm} , works in a cooperative manner with a Hill coefficient of 2. Complete model details can be found in Sneyd et al. (2003).

In summary,

$$J_{\text{pm}} = \frac{V_{\text{pm}} c^2}{K_{\text{pm}}^2 + c^2}, \text{ plasma membrane calcium pump,} \quad (5)$$

$$J_{\text{mito}} = \frac{V_{\text{mito}} c}{1 + (1/c)^2}, \text{ mitochondrial uptake,} \quad (6)$$

$$J_{\text{serca}} = \left(\frac{V_{\text{serca}} c}{K_{\text{serca}} + c} \right) \left(\frac{1}{c_e} \right), \text{ SERCA pump,} \quad (7)$$

$$J_{\text{in}} = \alpha_1 + \alpha_2 p, \text{ influx from outside the cell,} \quad (8)$$

$$P_{\text{RyR}} = \frac{w(1 + (c/K_b)^3)}{1 + (K_a/c)^4 + (c/K_b)^3}, \text{ RyR open probability,} \quad (9)$$

$$P_{\text{IPR}} = (0.1 O + 0.9 A)^4, \text{ IPR open probability,} \quad (10)$$

$$w^\infty(c) = \frac{1 + (K_a/c)^4 + (c/K_b)^3}{1 + (1/K_c) + (K_a/c)^4 + (c/K_b)^3}, \quad (11)$$

$$\text{and } K_a^4 = k_a^-/k_a^+, K_b^3 = k_b^-/k_b^+, \text{ and } K_c = k_c^-/k_c^+.$$

Model 1

$$\frac{dc^{(i)}}{dt} = (k_f P_{\text{IPR}}^{(i)} + v_1 P_{\text{RyR}}^{(i)} + J_{\text{er}}^{(i)})(c_e^{(i)} - c^{(i)}) - J_{\text{serca}}^{(i)} + \delta(J_{\text{in}}^{(i)} - J_{\text{pm}}^{(i)}) + \varepsilon(c^{(i-1)} - 2c^{(i)} + c^{(i+1)}), \quad (12)$$

$$\frac{1}{\gamma} \frac{dc_e^{(i)}}{dt} = -(k_f P_{\text{IPR}}^{(i)} + v_1 P_{\text{RyR}}^{(i)} + J_{\text{er}}^{(i)})(c_e^{(i)} - c^{(i)}) + J_{\text{serca}}^{(i)}, \quad (13)$$

$$\frac{dR^{(i)}}{dt} = \phi_{-2} O^{(i)} - \phi_2 p^{(i)} R^{(i)} + (k_{-1} + l_{-2}) I_1^{(i)} - \phi_1 R^{(i)}, \quad (14)$$

$$\frac{dO^{(i)}}{dt} = \phi_2 p^{(i)} R^{(i)} - (\phi_{-2} + \phi_4 + \phi_3) O^{(i)} + \phi_{-4} A^{(i)} + k_{-3} S^{(i)}, \quad (15)$$

$$\frac{dA^{(i)}}{dt} = \phi_4 O^{(i)} - \phi_{-4} A^{(i)} - \phi_5 A^{(i)} + (k_{-1} + l_{-2}) I_2^{(i)}, \quad (16)$$

$$\frac{dI_1^{(i)}}{dt} = \phi_1 R^{(i)} - (k_{-1} + l_{-2}) I_1^{(i)}, \quad (17)$$

$$\frac{dI_2^{(i)}}{dt} = \phi_5 A^{(i)} - (k_{-1} + l_{-2}) I_2^{(i)}, \quad (18)$$

$$\frac{dw^{(i)}}{dt} = \frac{k_c^-(w^\infty(c^{(i)}) - w^{(i)})}{w^\infty(c^{(i)})}, \quad (19)$$

$$\frac{dp^{(i)}}{dt} = \beta(p_{\text{st}}^{(i)} - p^{(i)}), \quad (20)$$

where ε denotes the strength of coupling and the superscripts $i = 1, 2, 3$ denote the different cells.

The functions ϕ are given below for completeness. Their derivation can be found in Sneyd and Dufour (2002).

$$\phi_1(c) = \frac{(k_1 L_1 + l_2) c}{L_1 + c(1 + L_1/L_3)}, \quad (21)$$

$$\phi_2(c) = \frac{k_2 L_3 + l_4 c}{L_3 + c(1 + L_3/L_1)}, \quad (22)$$

$$\phi_{-2}(c) = \frac{k_{-2} + l_{-4} c}{1 + c/L_5}, \quad (23)$$

$$\phi_3(c) = \frac{k_3 L_5}{L_5 + c}, \quad (24)$$

$$\phi_4(c) = \frac{(k_4 L_5 + l_6)c}{L_5 + c}, \quad (25)$$

$$\phi_{-4}(c) = \frac{L_1(k_{-4} + l_{-6})}{L_1 + c}, \quad (26)$$

$$\phi_5(c) = \frac{(k_1 L_1 + l_2)c}{L_1 + c}, \quad (27)$$

where $l_{-2} = l_2 k_{-1}/k_1 L_1$, $l_{-4} = k_{-2} l_4/k_2 L_3$, and $l_{-6} = k_{-4} l_6/k_4 L_5$.

Model 2

This model uses the same reaction kinetics as Model 1 but assumes that Ca^{2+} and IP_3 are free to diffuse in a two-dimensional domain. Ca^{2+} in the ER is assumed not to diffuse, although relaxation of this assumption makes no change to our results (computations not shown). Thus we get the reaction-diffusion equations

$$\frac{dx_j^2}{dt} = f_j + \delta_{j1} \varepsilon (x_1^1 - 2x_1^2 + x_1^3), \quad (28)$$

$$\frac{\partial p}{\partial t} = D_p \nabla^2 p + \beta(p_{\text{st}} - p), \quad (29)$$

$$\frac{1}{\gamma} \frac{\partial c_e}{\partial t} = -(k_f P_{\text{IPR}} + v_1 P_{\text{RyR}} + J_{\text{er}})(c_e - c) + J_{\text{serca}}, \quad (30)$$

coupled to Eqs. 14–19 describing the dynamics of the IPR and RyR.

All the model parameters are given in Table 1.

APPENDIX 2: FACTORIZATION OF THE CHARACTERISTIC POLYNOMIAL FOR THREE COUPLED CELLS

The stability of the symmetric steady state of three interacting cells was analyzed by linearization of the system Eqs. 12–20 in the neighborhood of the symmetric steady state. Let us consider three identical cells, each containing a system of m differential equations for the variable species x_1^i, \dots, x_m^i , $i = 1, 2, 3$. The cells are coupled in nearest-neighbor manner by diffusion of one of these entities, e.g., x_1^i . The whole system dynamics is described by

$$\frac{dx_j^1}{dt} = f_j + \delta_{j1} \varepsilon (x_1^3 - 2x_1^1 + x_1^2), \quad (31)$$

$$\frac{dx_j^2}{dt} = f_j + \delta_{j1} \varepsilon (x_1^1 - 2x_1^2 + x_1^3), \quad (32)$$

$$\frac{dx_j^3}{dt} = f_j + \delta_{j1} \varepsilon (x_1^2 - 2x_1^3 + x_1^1). \quad (33)$$

The functions f_j describe the rate of change in the internal species, x_j^i , and δ_{j1} is the Kronecker symbol ($\delta_{j1} = 1$ for $j = 1$ and $\delta_{j1} = 0$ for $j \neq 1$) where $j = 1, \dots, m$, and $i = 1, 2, 3$; see Eqs. 12–20 for the case of Ca^{2+} dynamics in a pancreatic acinus. The total number of variables in the equation system (Eqs. 31–33) equals $3 \times m$.

We use the entities x_j^1 of the first cell and the differences $\Delta x_j^2 = x_j^2 - x_j^1$ and $\Delta x_j^3 = x_j^3 - x_j^1$ as a new complete set of variables. The symmetric steady state is characterized by equal values of the corresponding species in the

different cells; that is, by \bar{x}_j^1 and $\bar{\Delta x}_j^2 = 0$, and $\bar{\Delta x}_j^3 = 0$. For the stability analysis of this steady state, we consider a linearization of the differential equation system (Eqs. 31–33) in the neighborhood of this steady state with respect to the deviations $\sigma_j^1 = x_j^1 - \bar{x}_j^1$ and $\Delta_j^2 = \Delta x_j^2 - \bar{\Delta x}_j^2$, and $\Delta_j^3 = \Delta x_j^3 - \bar{\Delta x}_j^3$. In this way we obtain for the variables of the first cell and for the differences characterizing the variables of the other cells the system

$$\frac{d\sigma_j^1}{dt} = \sum_{k=1}^m \frac{\partial f_j}{\partial x_k^1} \sigma_k^1 + \delta_{j1} \varepsilon (\sigma_1^3 - 2\sigma_1^1 + \sigma_1^2), \quad (34)$$

$$\frac{d\Delta_j^2}{dt} = \sum_{k=1}^m \frac{\partial f_j}{\partial x_k^1} \Delta_k^2 - 3\delta_{j1} \varepsilon \Delta_1^2, \quad (35)$$

$$\frac{d\Delta_j^3}{dt} = \sum_{k=1}^m \frac{\partial f_j}{\partial x_k^1} \Delta_k^3 - 3\delta_{j1} \varepsilon \Delta_1^3, \quad (36)$$

where $j, k = 1, \dots, m$. In Eqs. 35 and 36, the identity of the cells is taken into account; that is, the derivatives $\partial f_j / \partial x_k^2 = \partial f_j / \partial x_k^1$ and $\partial f_j / \partial x_k^3 = \partial f_j / \partial x_k^1$ at the symmetric steady state are for all values of j and k , independent of the cell index number.

Further we introduce the mean values of the system entities as

$$\tilde{x}_j = \frac{1}{3}(x_j^1 + x_j^2 + x_j^3), \quad j = 1, \dots, m, \quad (37)$$

and the corresponding deviations from their steady-state values $\tilde{\tilde{x}}_j$,

$$\tilde{\sigma}_j = \tilde{x}_j - \tilde{\tilde{x}}_j = \frac{1}{3}(3\sigma_j^1 + \Delta_j^2 + \Delta_j^3), \quad j = 1, \dots, m. \quad (38)$$

In the latter equation the identity of the symmetric steady state, which directly implies that $\tilde{\tilde{x}}_j = \bar{x}_j^1$, is again taken into account.

We consider next the rates of changes for the deviations $\tilde{\sigma}_j$ of the mean intracellular species,

$$\frac{d\tilde{\sigma}_j}{dt} = \frac{1}{3} \left(3 \frac{d\sigma_j^1}{dt} + \frac{d\Delta_j^2}{dt} + \frac{d\Delta_j^3}{dt} \right) \quad j = 1, \dots, m.$$

Using Eqs. 34–36, one easily derives

$$\begin{aligned} \frac{d\tilde{\sigma}_j}{dt} = \frac{1}{3} \sum_{k=1}^m \frac{\partial f_j}{\partial x_k^1} (3\sigma_k^1 + \Delta_k^2 + \Delta_k^3) \\ - \delta_{j1} \varepsilon (-\sigma_1^3 + 2\sigma_1^1 - \sigma_1^2 + \Delta_1^2 + \Delta_1^3). \end{aligned} \quad (39)$$

With Eqs. 37 and 38, this equation system may be written as

$$\frac{d\tilde{\sigma}_j}{dt} = \sum_{k=1}^m \frac{\partial f_j}{\partial x_k^1} \tilde{\sigma}_k, \quad j = 1, \dots, m. \quad (40)$$

The linear equation system (Eq. 40) for the deviations $\tilde{\sigma}_j$ of the mean values of the intracellular species is identical with the linearized system of a single cell, containing the same variables. In particular it is decoupled from the linear systems in Eqs. 35 and 36 for the differences Δ_j^2 and Δ_j^3 . Similarly the equation systems in Eqs. 35 and 36 for the variable differences are independent of the mean values. In addition to that, each subsystem of Eqs. 35 and 36 characterized by a particular cell index number is decoupled from all other subsystems. These properties imply factorization of the characteristic polynomial for the eigenvalues as

$$F(\lambda) \times D(\lambda)^2 = 0,$$

where $F(\lambda)$ is the characteristic polynomial of degree m of the single cell and $D(\lambda)$ is the characteristic polynomial of degree m for any subsystem of the linear equation system in Eqs. 35 and 36.

J.S. and K.T.-A. were supported by the Marsden Fund of the Royal Society of New Zealand. D.Y. was supported by National Institutes of Health grants Nos. DE14756, DK54568, and P01-DE13539.

REFERENCES

- Ashby, M., M. Craske, M. Park, O. Gerasimenko, R. Burgoyne, O. Petersen, and A. Tepikin. 2002. Localised Ca^{2+} uncaging reveals polarised distribution of Ca^{2+} -sensitive Ca^{2+} release sites: mechanism of unidirectional Ca^{2+} waves. *J. Cell Biol.* 158:283–292.
- Ashwin, P., G. King, and W. Swift. 1990. Three identical oscillators with symmetric coupling. *Nonlinearity*. 3:585–601.
- Baesens, C., J. Guckenheimer, S. Kim, and R. MacKay. 1991. Three coupled oscillators: mode-locking, global bifurcations and toroidal chaos. *Phys. D*. 49:387–475.
- Berridge, M., and G. Dupont. 1994. Spatial and temporal signalling by calcium. *Curr. Opin. Cell Biol. Rev.* 6:267–274.
- Cancela, J. 2001. Specific Ca^{2+} signalling evoked by cholecystokinin and acetylcholine: The roles of NAADP, cADPR, and IP_3 . *Annu. Rev. Physiol.* 63:99–117.
- Cancela, J., F. Van Coppenolle, A. Galione, A. Tepikin, and O. Petersen. 2002. Transformation of local Ca^{2+} spikes to global Ca^{2+} transients: the combinatorial roles of multiple Ca^{2+} releasing messengers. *EMBO J.* 21:909–919.
- Clair, C., C. Chalumeau, T. Tordjmann, J. Poggioli, C. Erneux, G. Dupont, and L. Combettes. 2001. Investigation of the roles of Ca^{2+} and InsP_3 diffusion in the coordination of Ca^{2+} signals between connected hepatocytes. *J. Cell Sci.* 114:1999–2007.
- Doedel, E., A. Champneys, T. Fairgrieve, Y. Kuznetsov, B. Sandstede, and X. Wang. 1997. AUTO97: continuation and bifurcation software for ordinary differential equations (with HomCont). Technical report. Concordia University, Montreal, Canada.
- Dupont, G., S. Swillens, C. Clair, T. Tordjmann, and L. Combettes. 2000a. Hierarchical organization of calcium signals in hepatocytes: from experiments to models. *Biochim. Biophys. Acta.* 1498:134–152.
- Dupont, G., T. Tordjmann, C. Clair, S. Swillens, M. Claret, and L. Combettes. 2000b. Mechanism of receptor-oriented intercellular calcium wave propagation in hepatocytes. *FASEB J.* 14:279–289.
- Ermentrout, B. 2002. Simulating, Analyzing and Animating Dynamical Systems: A Guide to XPPAUT for Researchers and Students. SIAM, Philadelphia, PA.
- Fogarty, K., J. Kidd, D. Tuft, and P. Thorn. 2000a. A bimodal pattern of InsP_3 -evoked elementary Ca^{2+} signals in pancreatic acinar cells. *Biophys. J.* 78:2298–2306.
- Fogarty, K., J. Kidd, D. Tuft, and P. Thorn. 2000b. Mechanisms underlying InsP_3 -evoked global Ca^{2+} signals in mouse pancreatic acinar cells. *J. Physiol. (Lond.)*. 526:515–526.
- Giaume, C., and L. Venance. 1998. Intercellular calcium signaling and gap junctional communication in astrocytes. *Glia*. 24:50–64.
- Golubitsky, M., and I. Stewart. 2002. The symmetry perspective. In *Equilibrium to Chaos in Phase Space and Physical Space*. Birkhäuser Verlag, Basel, Taschenbuch, Switzerland.
- Höfer, T. 1999. Model of intercellular calcium oscillations in hepatocytes: synchronization of heterogeneous cells. *Biophys. J.* 77:1244–1256.
- Höfer, T., A. Politi, and R. Heinrich. 2001. Intercellular Ca^{2+} wave propagation through gap-junctional Ca^{2+} diffusion: a theoretical study. *Biophys. J.* 80:75–87.
- Höfer, T., L. Venance, and C. Giaume. 2002. Control and plasticity of intercellular calcium waves in astrocytes: a modeling approach. *J. Neurosci.* 22:4850–4859.
- Kasai, H. 1995. Pancreatic calcium waves and secretion. *CIBA Found. Symp.* 188:104–116.
- Kasai, H., Y.-X. Li, and Y. Miyashita. 1993. Subcellular distribution of Ca^{2+} release channels underlying Ca^{2+} waves and oscillations in exocrine pancreas. *Cell*. 74:669–677.
- Keizer, J., and L. Levine. 1996. Ryanodine receptor adaptation and Ca^{2+} -induced Ca^{2+} release-dependent Ca^{2+} oscillations. *Biophys. J.* 71:3477–3487.
- Lawrie, A., E. Toescu, and D. Gallacher. 1993. Two different spatiotemporal patterns for Ca^{2+} oscillations in pancreatic acinar cells: evidence of a role for protein kinase C in $\text{Ins}(1,4,5)\text{P}_3$ -mediated Ca^{2+} signalling. *Cell Calcium*. 14:698–710.
- Leite, M., A. Burgstahler, and M. Nathanson. 2002. Ca^{2+} waves require sequential activation of inositol trisphosphate receptors and ryanodine receptors in pancreatic acini. *Gastroenterology*. 122:415–427.
- Nathanson, M., P. Padfield, A. O'Sullivan, A. Burgstahler, and J. Jamieson. 1992. Mechanism of Ca^{2+} wave propagation in pancreatic acinar cells. *J. Biol. Chem.* 267:18118–18121.
- Ngezhayao, A., and H.-A. Kolb. 1993. Gap junctional conductance tunes phase differences of cholecystokinin-evoked calcium oscillations in pairs of pancreatic acinar cells. *Pflügers Arch.* 422:413–415.
- Petersen, C., and O. Petersen. 1991. Receptor-activated cytoplasmic Ca^{2+} spikes in communicating cluster of pancreatic acinar cells. *FEBS Lett.* 284:113–116.
- Robb-Gaspers, L., and A. Thomas. 1995. Coordination of Ca^{2+} signaling by intercellular propagation of Ca^{2+} waves in the intact liver. *J. Biol. Chem.* 270:8102–8107.
- Sanderson, M. 1995. Intercellular calcium waves mediated by inositol trisphosphate. *CIBA Found. Symp.* 188:175–189.
- Sneyd, J., and J. Dufour. 2002. A dynamic model of the type-2 inositol trisphosphate receptor. *Proc. Natl. Acad. Sci. USA*. 99:2398–2403.
- Sneyd, J., B. Wetton, A. Charles, and M. Sanderson. 1995. Intercellular calcium waves mediated by the diffusion of inositol trisphosphate: a two-dimensional model. *Am. J. Physiol. Cell Physiol.* 268:C293–C302.
- Sneyd, J., M. Wilkins, A. Strahonja, and M. Sanderson. 1998. Calcium waves and oscillations driven by an intercellular gradient of inositol (1,4,5)-trisphosphate. *Biophys. Chem.* 72:101–109.
- Sneyd, J., K. Tsaneva-Atanasova, J. Bruce, S. Straub, D. Giovannucci, and D. Yule. 2003. A model of calcium waves in pancreatic and parotid acinar cells. *Biophys. J.* 85:1392–1405.
- Stauffer, P., H. Zhao, K. Luby-Phelps, R. Moss, R. Star, and S. Muallem. 1993. Gap junctional communication modulates $[\text{Ca}^{2+}]_i$ oscillations and enzyme secretion in pancreatic acini. *J. Biol. Chem.* 268:19769–19775.
- Straub, S., D. Giovannucci, and D. Yule. 2000. Calcium wave propagation in pancreatic acinar cells: functional interaction of inositol 1,4,5-trisphosphate receptors, ryanodine receptors, and mitochondria. *J. Gen. Physiol.* 116:547–560.
- Strogatz, S., and I. Stewart. 1993. Coupled oscillators and biological synchronization. *Sci. Am.* 269:102–108.
- Takamatsu, A., R. Tanaka, H. Yamada, T. Nakagaki, T. Fujii, T., and I. Endo. 2001. Spatiotemporal symmetry in rings of coupled biological oscillators of *Physarum* plasmodial slime mold. *Phys. Rev. Lett.* 87:078102–1–078102-4.
- Thomas, A., D. Renard-Rooney, G. Hajnoczky, L. Robb-Gaspers, C. Lin, and T. Rooney. 1995. Subcellular organization of calcium signalling in hepatocytes and the intact liver. *CIBA Found. Symp.* 188:18–35.
- Thorn, P. 1996. Spatial domains of Ca^{2+} signalling in secretory epithelial cells. *Cell Calcium*. 20:203–214.
- Thorn, P., A. Lawrie, P. Smith, D. Gallacher, and O. Petersen. 1993b. Local and global cytosolic Ca^{2+} oscillations in exocrine cells evoked by agonists and inositol trisphosphate. *Cell*. 74:661–668.

- Tinel, H., J. Cancela, H. Mogami, J. Gerasimenko, O. Gerasimenko, A. Tepikin, and O. Petersen. 1999. Active mitochondria surrounding the pancreatic acinar granule region prevent spreading of inositol triphosphate-evoked local cytosolic Ca^{2+} signals. *EMBO J.* 18:4999–5008.
- Wäsele, B., and J. Edwardson. 2002. The regulation of exocytosis in the pancreatic acinar cell. *Cell. Signal.* 14:191–197.
- Wolf, J., and R. Heinrich. 1997. Dynamics of two-component biochemical system in interacting cells; synchronization and desynchronization of oscillations and multiple steady states. *BioSystems.* 43:1–24.
- Yoshimoto, M., K. Yoshikawa, and Y. Mori. 1993. Coupling among three chemical oscillators: synchronization, phase death, and frustration. *Phys. Rev. E.* 47:864–874.
- Yule, D., A. Lawrie, and D. Gallacher. 1991. Acetylcholine and cholecystokinin induce different patterns of oscillating calcium signals in pancreatic acinar cells. *Cell Calcium.* 12:145–151.
- Yule, D., E. Stuenkel, and J. Williams. 1996. Intercellular calcium waves in rat pancreatic acini: mechanism of transmission. *Am. J. Physiol.* 271: C1285–C1294.